Physica A 387 (2008) 6263–6276

Contents lists available at ScienceDirect

Physica A

journal homepage: www.elsevier.com/locate/physa

Analysis of stresses in two-dimensional isostatic granular systems

Margot Gerritsen [a,*], Gunilla Kreiss [b], Raphael Blumenfeld [c,d]

[a] Stanford University, Department of Energy Resources Engineering, Stanford, CA 94305-2220, USA
[b] University of Uppsala, Department of Information Technology, 75108 Uppsala, Sweden
[c] Imperial College, Earth Science and Engineering, London SW7 2AZ, UK
[d] Cambridge University, Cavendish Laboratory, Cambridge CB3 0HE, UK

ARTICLE INFO

Article history:
Received 27 April 2008
Received in revised form 17 June 2008
Available online 12 July 2008

Keywords:
Granular systems
Stress
Isostaticity theory
Force chains

ABSTRACT

We analyze a recently proposed continuous model for stress fields that develop in two-dimensional purely isostatic granular systems. We present a reformulation of the field equations, as a linear first-order hyperbolic system, and show that it is very convenient both for analysis and for numerical computations. Our analysis allows us to predict quantitatively the formation and directions of stress paths and, from these, trajectories and magnitudes of force chains, given the structure in terms of a particular fabric tensor. We further predict quantitatively changes of stresses along the paths, as well as leakage and branching of stress from the main paths into the cones that they make in terms of the fabric tensor. Numerical computations in both Cartesian and cylindrical coordinates verify the analytic results and illustrate the rich behavior discovered. All the phenomena predicted by our solutions have been observed experimentally, suggesting that stresses in isostatic systems can form a base model for a more developed stress theory in granular materials.

1. Introduction

Granular materials, such as gravel, beans, agricultural grains and seeds, and powders, play a dominant role in everyday life [1]. It is often observed that stress transmission in these materials is markedly different than a priori predictions of conventional elasticity theory. Of particular interest are common observations of emergence of 'force chains' and 'arches' [2,3]. It has been suggested that this is because real cohesionless granular materials are in fact two-phase composites – part isostatic and part overconnected [4,5]. How close a granular pack is to being isostatic depends on several factors, such as grain rigidity and connectivity at the granular level [4,7], but this issue is outside the main thrust of this paper. To develop this picture further and model stress transmission in real materials, it is therefore important to understand first how stresses develop in each of the pure phases separately. The aim of this paper is to study in detail the response in the purely isostatic phase, when the structure varies nonuniformly with position. The continuous equations of isostatic materials, given in detail below, were first proposed on empirical basis in the mid 90s [8] and have been derived later from basic principles in two-dimensional (2D) systems on the scale of very few grains [9]. In a further development, a procedure was constructed to upscale the 2D equations to mesoscopic scales [10].

In this paper, we first reformulate the fundamental equations as a first-order hyperbolic system in a way that makes possible a convenient analysis. This form allows us to gain insight into, and predict quantitatively, the rich patterns of stresses that develop in purely isostatic granular systems. In particular, we shed light on a range of stress solutions and make

* Corresponding author. Tel.: +1 650 725 2727; fax: +1 650 725 2099.
E-mail addresses: margot.gerritsen@stanford.edu (M. Gerritsen), gunilla.kreiss@it.uu.se (G. Kreiss), rbb11@cam.ac.uk (R. Blumenfeld).

0378-4371/$ – see front matter © 2008 Elsevier B.V. All rights reserved.
doi:10.1016/j.physa.2008.06.057

quantitative prediction on phenomena: force chain coning and meandering, growth/decay of stresses along chains, leakage from force chains, branching of chains and non-interference of force chain cones from one another. Most importantly, we show that predictions about stress patterns and branching can be made directly from the stress equations without resorting to further models or ad hoc assumptions. We demonstrate a range of non-uniform stress solutions by exact and numerical analyses.

1.1. Stress equations for isostatic systems

Assemblies of grains are isostatic, or statically determinate, when the inter-granular forces can be fully determined from statics, namely, from balance of forces and torque moments. To be isostatic, a pack of infinitely rigid grains has only to satisfy the condition that the mean number of force-carrying contacts per grain has a particular value. This value depends on the dimensionality of the system, on inter-granular friction and to some extent on the shape of the particles [6].

In two dimensions, the balance conditions for static stress are given by two force equations

$$\partial_x \sigma_{xx} + \partial_y \sigma_{yx} = g_x \tag{1}$$

$$\partial_x \sigma_{xy} + \partial \sigma_{yy} = g_y, \tag{2}$$

in the x- and y-directions, respectively, and one global torque moment condition,

$$\sigma_{xy} = \sigma_{yx}, \tag{3}$$

where σ_{ij} are the elements of the symmetric stress tensor Σ

$$\Sigma = \begin{pmatrix} \sigma_{xx} & \sigma_{xy} \\ \sigma_{xy} & \sigma_{yy} \end{pmatrix}. \tag{4}$$

In Eqs. (1) and (2), g_x and g_y are the components of an external force field $\vec{g}$ that may include body forces. It has been shown in Refs. [9,10] that in isostaticity theory the equations are closed by the relation

$$p_{xx}\sigma_{yy} + p_{yy}\sigma_{xx} = 2p_{xy}\sigma_{xy}, \tag{5}$$

which originates from the condition of local torque balance. The parameters p_{ij} are the elements of the symmetric fabric tensor P,

$$P = \begin{pmatrix} p_{xx} & p_{xy} \\ p_{xy} & p_{yy} \end{pmatrix},$$

that characterizes the local structure. This fabric tensor has been defined explicitly in terms of the structure around grains in Refs. [4,9], where it was also identified as a measure of the rotational disorder around grains. A detailed consideration of the geometric interpretation of P and its statistical properties has shown that, on the coarse-grained scale that the equations apply, the determinant of the fabric tensor is negative, $\det(P) < 0$, regardless of structural correlations or anisotropy [4]. This is an important finding that substantiates a previous suggestion, made on empirical grounds [8], that the stress equations of isostatic granular systems are hyperbolic, as will be detailed below.

The above equations were analyzed in Ref. [5], by decoupling them into scalar integro-differential equations for the individual stress components, σ_{ij}. Although that decoupling enabled analysis of solutions for constant fabric tensors, it is not an attractive formulation for more general cases.

In this work we:

- reformulate the field equations as a strictly hyperbolic first-order system, both in Cartesian and in cylindrical coordinates;
- show that the reformulation makes possible the general calculation of stress paths (force chains), both for constant and variable fabric tensors;
- show that the reformulation gives novel insight into the behavior of stresses in isostatic systems and, for variable fabric tensors, we use it to predict meandering stress chains, coning, stress growth or decay along chains, intra-cone leakage and stress chain branching;
- derive explicit solutions for variable fabric tensors using a perturbation analysis.

We support our analytical results by numerical solutions, obtained with a third-order Essentially Non-Oscillatory discretization of the hyperbolic system, combined with a third-order Runge–Kutta time-stepping method [11]. All results shown are converged solutions for a large number of grid points to exclude any numerical biasing.

The paper is organized as follows: In Section 2 we reformulate the isostatic stress equations in Cartesian coordinates as a first-order hyperbolic system. Sections 3 and 4 analyze the cases of constant and variable fabric tensor, respectively. In particular, mechanisms for stress chains, stress leakage, stress coning, growth, decay and branching are identified and discussed. In Section 5 we present the system of equations in cylindrical coordinates. A perturbation expansion is introduced in Section 6, which allows for analysis of the phenomena identified in Sections 3 and 4. The paper concludes with a discussion of the results and future work in Section 7.

2. Derivation of the hyperbolic system of stress equations in Cartesian coordinates

Let us consider first the case $p_{xx} \neq 0$. At the end of this section we comment on the special cases, when one or more of the components of P vanish. We can rewrite Eq. (5) as

$$\sigma_{yy} = 2q_{xy}\sigma_{xy} - q_{yy}\sigma_{xx}, \quad \text{with } q_{xy} = \frac{p_{xy}}{p_{xx}},\ q_{yy} = \frac{p_{yy}}{p_{xx}}. \tag{6}$$

Introducing

$$\vec{u} = \begin{pmatrix} \sigma_{xx} \\ \sigma_{xy} \end{pmatrix},$$

and substituting Eq. (6) in Eq. (2), we rewrite Eqs. (1) and (2) as

$$\partial_x \vec{u} + \partial_y (A\vec{u}) = \vec{g}, \quad \text{with } A = \begin{pmatrix} 0 & 1 \\ -q_{yy} & 2q_{xy} \end{pmatrix}, \qquad \vec{g} = \begin{pmatrix} g_x \\ g_y \end{pmatrix}. \tag{7}$$

The eigenvalues of the matrix A satisfy the characteristic equation

$$-\lambda(2q_{xy} - \lambda) + q_{yy} = 0,$$

and are given by

$$\lambda_{1,2} = q_{xy} \pm \sqrt{q_{xy}^2 - q_{yy}}.$$

Since $\det(P) < 0$ then $q_{xy}^2 - q_{yy} = -\det(P)/p_{xx}^2 > 0$, and the eigenvalues λ_i are distinct and real, making system (7) strictly hyperbolic. It is well known how to formulate boundary conditions to such equations that ensure well-posedness, as is discussed in Ref. [13].

The matrix A can be diagonalized as $A = Y\Lambda Y^{-1}$, with

$$Y = \begin{pmatrix} 1 & 1 \\ \lambda_1 & \lambda_2 \end{pmatrix}, \qquad Y^{-1} = \frac{1}{\lambda_2 - \lambda_1} \begin{pmatrix} \lambda_2 & -1 \\ -\lambda_1 & 1 \end{pmatrix}, \quad \text{and} \quad \Lambda = \begin{pmatrix} \lambda_1 & 0 \\ 0 & \lambda_2 \end{pmatrix}. \tag{8}$$

The columns $\vec{y}_i$ of the matrix Y are the eigenvectors of A. Introduce the characteristic variables w_1 and w_2,

$$\vec{w} = \begin{pmatrix} w_1 \\ w_2 \end{pmatrix} = Y^{-1}\vec{u} = \frac{1}{\lambda_2 - \lambda_1} \begin{pmatrix} \lambda_2\sigma_{xx} - \sigma_{xy} \\ -\lambda_1\sigma_{xx} + \sigma_{xy} \end{pmatrix}, \tag{9}$$

and substituting them into (7), yields the system of equations

$$\partial_x \vec{w} + \Lambda\partial_y \vec{w} = \vec{h} + (B - \partial_y \Lambda)\vec{w}, \tag{10}$$

where

$$\vec{h} = Y^{-1}\vec{g}, \quad \text{and} \quad B = -Y^{-1}\left(\partial_x Y + \partial_y Y \Lambda\right).$$

Since $\vec{h}$ is independent of $\vec{w}$ and Λ is diagonal then the equations for w_1 and w_2 in (10) are coupled only through the term containing B. The matrix B is singular and it has the form

$$B = \frac{-1}{\lambda_1 - \lambda_2} \begin{pmatrix} \partial_x\lambda_1 + \lambda_1\partial_y\lambda_1 & \partial_x\lambda_2 + \lambda_2\partial_y\lambda_2 \\ -\partial_x\lambda_1 - \lambda_1\partial_y\lambda_1 & -\partial_x\lambda_2 - \lambda_2\partial_y\lambda_2 \end{pmatrix}. \tag{11}$$

Significantly, note that B vanishes when the fabric tensor P is constant as a function of position.

The stress tensor Σ, given by Eq. (4), can be expressed in the characteristic variables by substitution of Eqs. (9) and (6),

$$\Sigma = w_1 \begin{pmatrix} 1 & \lambda_1 \\ \lambda_1 & \lambda_1^2 \end{pmatrix} + w_2 \begin{pmatrix} 1 & \lambda_2 \\ \lambda_2 & \lambda_2^2 \end{pmatrix}. \tag{12}$$

To obtain a well-posed problem we must augment the system of equations with suitable boundary conditions. If the system (7) is valid for $(x, y) \in \Omega$, then, by standard theory for hyperbolic systems, the Dirichlet conditions for stresses should be given so that for each characteristic in Ω the corresponding characteristic variable is prescribed at exactly one boundary point. For example, if the domain is $0 \leq x \leq X,\ -\infty < y < \infty$ we can use a boundary condition of the form

$$\overrightarrow{u}(0, y) = \vec{f}(y). \tag{13}$$

For completeness, we comment that when p_{xx} vanishes the solution of the equations is considerably simplified and the results remain qualitatively the same, if not in details. This is also the case when both p_{xx} and p_{yy} vanish. p_{xx} and p_{xy} cannot vanish simultaneously without violating the assumption that $\det(P) < 0$.

3. Constant fabric tensors in Cartesian coordinates

If the fabric tensor is constant throughout the domain, both B and $\partial_y \Lambda$ vanish and the system of Eq. (10) decouples into two separate equations, one for each characteristic variable:

$$\partial_x w_i + \lambda_i \partial_y w_i = h_i, \quad i = 1, 2. \tag{14}$$

In the following subsection, we analyze briefly the solutions for this case.

3.1. Stress propagation paths

We define the characteristic paths as the paths parameterized by a variable s through

$$\frac{\mathrm{d}x}{\mathrm{d}s} = 1 \qquad \frac{\mathrm{d}y}{\mathrm{d}s} = \lambda_i, \quad i = 1, 2. \tag{15}$$

The directions of the characteristic paths are given by the eigenvectors $y_i = \begin{bmatrix} 1 \\ \lambda_i \end{bmatrix}$ of A. Eq. (15) can now be written as the ordinary differential equations

$$\frac{\mathrm{d}w_i}{\mathrm{d}s} = h_i \quad i = 1, 2, \tag{16}$$

along the characteristic paths, which for constant fabric tensors are straight lines.

Consider the semi-infinite plane $x \geq 0, -\infty \leq y \leq \infty$. At each point $(\widetilde{x}, \widetilde{y})$, the characteristic variables $\vec{w}$ can be computed by integrating Eq. (16), each along its unique characteristic path,

$$w_i(\widetilde{x}, \widetilde{y}) = w_i(0, \widetilde{y} - \lambda_i \widetilde{x}) + \int_0^{\widetilde{x}} h_i(s)\mathrm{d}s, \quad i = 1, 2.$$

The stresses σ_{xx} and σ_{xy} at $(\widetilde{x}, \widetilde{y})$ are then given by

$$\vec{u}(\widetilde{x}, \widetilde{y}) = \begin{bmatrix} \sigma_{xx}(\widetilde{x}, \widetilde{y}) \\ \sigma_{xy}(\widetilde{x}, \widetilde{y}) \end{bmatrix} = Y \vec{w}(\widetilde{x}, \widetilde{y}).$$

The remaining stress is determined through Eqs. (3) and (5).

The physical interpretation of this solution is that a localized stress, applied at any point $(0, y)$ along the boundary of the domain, 'propagates into' the domain along the two characteristic paths emanating from y. Therefore, the characteristic lines are also stress propagation paths. These solutions are in agreement with the stress chains found in Refs. [4,5].

Since $q_{yy} < 0$, the eigenvalues of A always have opposite signs and therefore, in our chosen coordinate systems, the stress paths have gradients of opposite signs. For $q_{yy} = -1$, the matrix A is symmetric, its eigenvectors are orthogonal and hence the stress paths are orthogonal as well.

In the following numerical solutions of Eq. (7), we take x to be the marching, or time-like, variable. That is, we first discretize in y and then solve the resulting system of ordinary differential equations in x. Note, that x can be the marching variable as long as $p_{xx} \neq 0$.

In Fig. 1, we illustrate the above analysis by solving for an arbitrary artificial constant fabric tensor

$$P_c = \begin{pmatrix} 1 & \frac{1}{2} \\ \frac{1}{2} & -3 \end{pmatrix}, \tag{17}$$

when a narrow Gaussian-shaped stress s_{xx} is applied at three different positions along the boundary $x = 0$. In Fig. 1a we show that the two characteristic paths from each source share the $\sigma_{xx}(0, y) = s_{xx}$ boundary load from that source, as determined by Eq. (9). Specifically, along each w_1-path $\sigma_{xx} = \frac{\lambda_2}{\lambda_2 - \lambda_1} s_{xx}$ while $\sigma_{xx} = \frac{\lambda_1}{\lambda_1 - \lambda_2} s_{xx}$ along each w_2-path. Because $\lambda_1 > 0$ and $\lambda_2 < 0$, both these fractions are always positive. It is important to note that, although no shear stress σ_{xy} is applied at the boundary, σ_{xy} is nevertheless nonzero along the characteristic paths. Here, $\sigma_{xy} = \frac{\lambda_1 \lambda_2}{\lambda_2 - \lambda_1} s_{xx}$ along the w_1-path and equal in magnitude but opposite in sign along the w_2-path. The figure also illustrates the superposition of the stress paths due to the linear character of the governing system of equations.

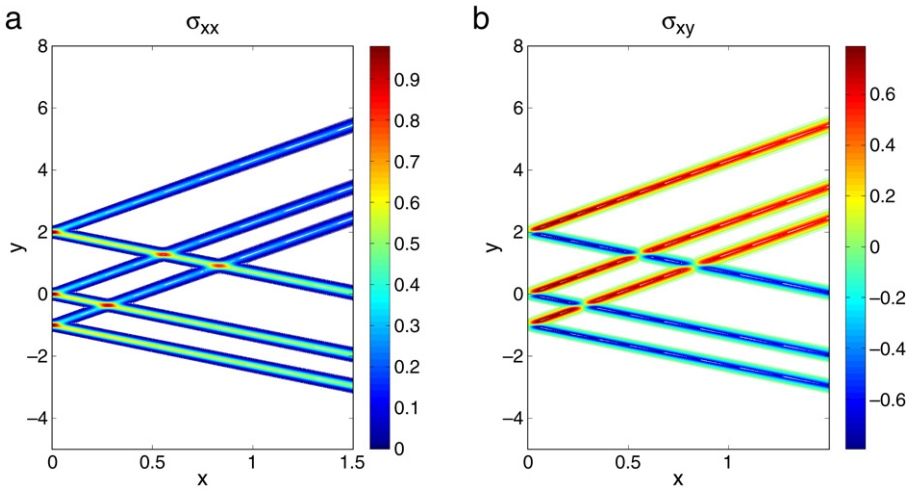

Fig. 1. Contour plots of (a) σ_{xx} and (b) σ_{xy}, when narrow Gaussian-shaped stresses s_{xx} are applied at three different positions along the boundary $x = 0$.

3.2. Principal stresses

The principal stresses of the stress tensor Σ in Eq. (12) are the eigenvalues of Σ, given by

$$\sigma_{\max,\min} = -\frac{\mathrm{Tr}(\Sigma)}{2} \pm \frac{1}{2}\sqrt{\mathrm{Tr}(\Sigma)^2 - 4\det(\Sigma)}, \tag{18}$$

with $\mathrm{Tr}(\Sigma) = w_1(1+\lambda_1^2) + w_2(1+\lambda_2^2)$ and $\det(\Sigma) = w_1 w_2(\lambda_1 - \lambda_2)^2$. It is instructive to compute the principal stresses along the characteristic paths. Inspection of (18) shows that, for any point along a stress path w_i on which all other incident characteristics have vanishing values of w, the stress tensor is singular and the principal stresses are $\sigma_{\min} = 0$ and $\sigma_{\max} = w_i\left(1+\lambda_i^2\right)$.

The principal stresses align with the eigenvectors of Σ and we find that the (normalized) eigenvector corresponding to $\sigma_{\max}$ is $[1, \lambda_i]/\sqrt{1+\lambda_i^2}$. Significantly, this coincides with the direction of the stress path. Thus, the direction of maximal stress is aligned with the stress path direction, in contrast to an earlier statement [5].

In regions where more than one characteristic variable are finite, the principal stresses are determined by contributions from several paths. In particular, in Fig. 2, we show a numerical computation of stress ellipses, for the constant fabric tensor given by Eq. (17), near (0, 0), where both paths contribute to the principal stresses. The local directions and lengths of the semi-major and semi-minor axes of a stress ellipse coincide, respectively, with the stress principal axes and the local maximum and minimum principal stresses. The principal stresses are normalized by the maximum principal stress at the boundary, s_{xx}. The stress ellipses are drawn on top of the contour plot of σ_{xx} for comparison.

The coincidence of the maximal stress principal axis with the path direction is in agreement with experimental observations of long force chains [2,3]. It is therefore plausible that these solutions describe the experimentally observed force chains. The vanishing of the minimal stress perpendicular to the main stress path is also significant – it underpins the fragility of stress paths [8], an issue that is beyond the scope of this paper and will be discussed elsewhere.

4. Variable fabric tensors in Cartesian coordinates

When the fabric tensor varies as a function of position, the characteristic variables are given by the generally coupled Eq. (10):

$$\partial_x w_i + \lambda_i \partial_y w_i = h_i - \partial_y \lambda_i w_i + (B\vec{w})_i\,, \quad i = 1, 2. \tag{19}$$

As above, stresses propagate along characteristic paths defined by (15), but the eigenvalues λ_i now vary as functions of position. Consequently, the stress paths are no longer straight and Eq. (15) must be integrated explicitly to find the trajectories. At each point in the domain, the stress paths align with the eigenvectors of the local Jacobian matrix A. In Fig. 3 we show solutions for a domain whose fabric tensor has the form

$$P = \begin{pmatrix} 1 & 2 \\ 2 & -1 \end{pmatrix} + \varepsilon \cos(2\pi x) \begin{pmatrix} 1 & 1 \\ 1 & 1 \end{pmatrix}, \tag{20}$$

with ε a small parameter, when a narrow Gaussian-shaped σ_{xy} load is applied around (0, 0). The fabric tensor in (20), is artificial and arbitrary, chosen to illustrate clearly the direct effect of the structure on the stress field. This comment applies

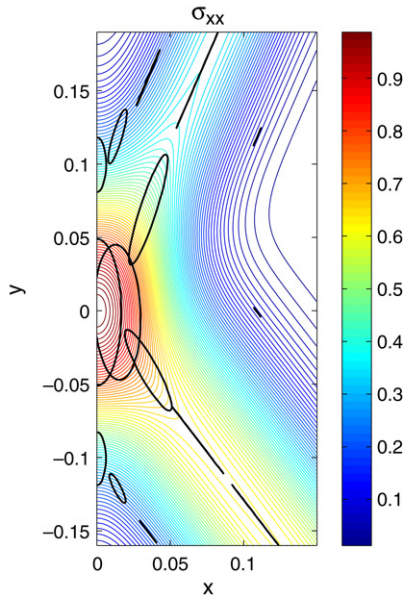

Fig. 2. Principal stress directions.

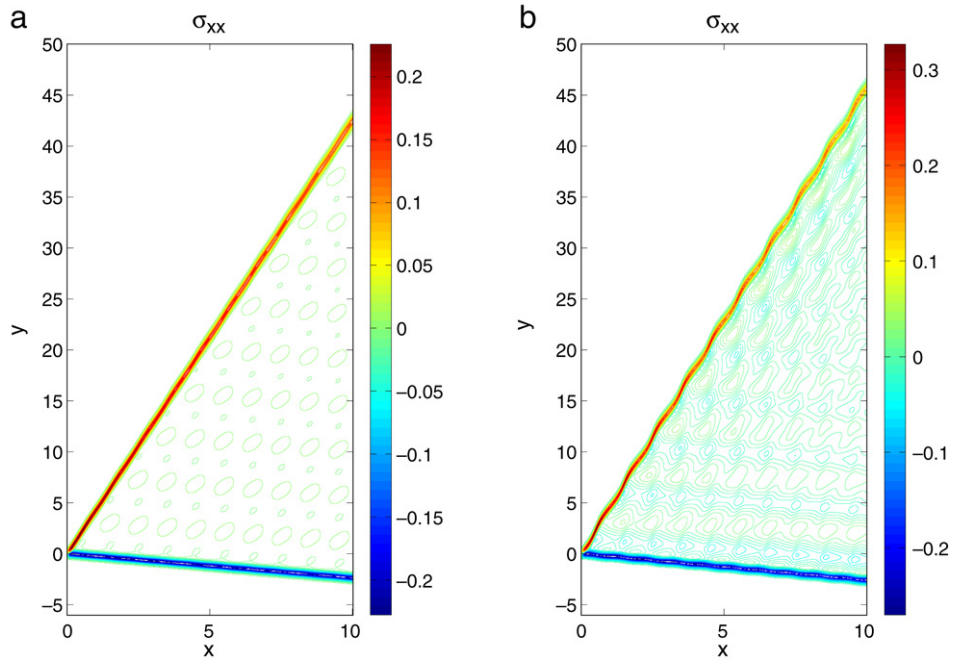

Fig. 3. Contour plots of σ_{xx} for the variable fabric tensor given by Eq. (20) when a narrow Gaussian-shaped stress σ_{xy} is applied at (0, 0): (a) $\varepsilon = 0.1$, weak variations in P and B; (b) $\varepsilon = 0.5$, stronger variations in P and B.

to all the explicit fabric tensors used in the following. It can be observed that the boundary stress is supported by two stress paths that waiver slightly about straight lines. Note that the periodicity of P gives rise to periodic waivering of the two main stress paths, as well as to a periodic stress pattern between them.

The right-hand side of Eq. (19) can be grouped into three parts, each giving rise to a different physical effect. The first, h_i, is independent of the stress field and can be regarded as an external source. The second group is $\left(B_{ii} - \partial_y \lambda_i\right) w_i$. This term can be immediately recognized to lead to an increase (decrease) of w_i where it is positive (negative). It is possible for any particular stress component to increase locally along a stress path, subject to specifiable constraints on the stresses both along the path and along the sub-branches leaking from it (see below). Over distances, however, stresses must attenuate. A detailed discussion of this issue is beyond the scope of this paper and will be given elsewhere.

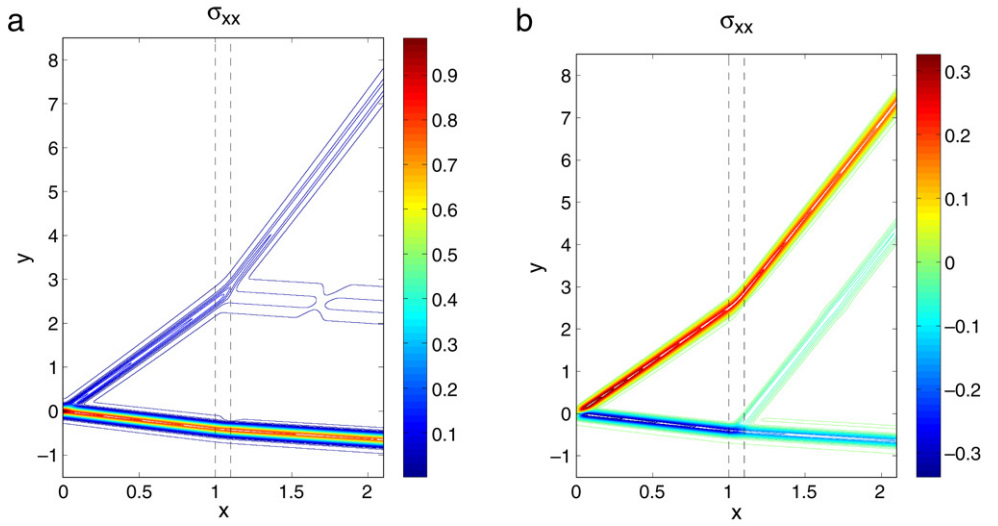

Fig. 4. Branching of stress paths resulting from a narrow Gaussian σ_{xx} applied at the boundary point (0, 0), as a result of strong gradients in P in the thin mid-layer between the dashed lines. (a) Contour plot for σ_{xy}; (b) Contour plot for σ_{xx}.

The third group consists of the off-diagonal terms in B and are the only terms that couple between the two characteristic paths. We demonstrate the change of the stresses along the paths in Fig. 3(b) for $\varepsilon = 0.5$. The coupling between the characteristics, caused by the third group, gives rise to 'leakage' from the stress paths into the cone of influence. As expected, there is no leakage to the outside of the cone of influence. The larger the gradients of P the stronger the coupling between the w_i and, indeed, both leakage from, and attenuation/growth along, the main stress paths are magnified from Fig. 3(a) to Fig. 3(b).

Large and localized gradients of P concentrate leakage at distinct points along the paths, giving rise to branch-like stress patterns oriented along the characteristic directions. This phenomenon is illustrated in the numerical solution shown in Fig. 4, where the path of a localized load σ_{xx} travels through three layers. In all three layers the diagonal elements of P are constant and identical: $p_{xx} = 1$ and $p_{yy} = -1$. The regions differ, however, in the off-diagonal element p_{xy}, which varies linearly in x. In layers 1, 2, and 3, the variations are $\mathrm{d}p_{xy}/\mathrm{d}x = 0.1, 4$ and 0.1, respectively. The small gradients in P in layers 1 and 3 do not give rise to any discernible leakage. In contrast, the large gradient of P in the thin mid-layer effects strong leakage that manifests itself as a branch in the stress path. It should be emphasized that branching is a special case of leakage when stress paths cross regions of sharp gradients of the fabric tensor P. Thus, experimental observations of branches depend not only on force thresholding [3], but also on exact nature of local variations of the fabric tensor.

Non-straight stress chains, leakage and branching have indeed been observed in a number of experiments [3]. However, it should be kept in mind that in most experiments the granular materials are not ideally isostatic, as discussed elsewhere [4], and therefore that the experimental support for our results, as well as for isostaticity theory in general, is tentative at this stage. Experimental data for purely isostatic systems are currently being planned to test these effects [12].

5. The stress equations in cylindrical coordinates

Many experiments are carried out in cylindrical geometries, e.g. Ref. [3]. This geometry is especially popular in an annulus setup, where the granular material is confined between two circular boundaries at $r = r_0$ and $r = r_1 > r_0$. Applying a small radial compressive stress, σ_{rr}, and rotating one of the boundaries with respect to the other, gives rise to a shear stress $\sigma_{r\theta}$. In such experiments, the stress is not applied uniformly across the boundary, but rather at particular points on relatively protruding grains. This generates a set of localized loads at points along the circular boundary (say at $r = r_0$) that act as load sources for our analysis.

In the following, we assume that the system is at rest under one such a localized load, applied at (r_0, θ_0) on the inner circular boundary. The symmetric stress tensor is

$$\Sigma = \begin{pmatrix} \sigma_{rr} & \sigma_{r\theta} \\ \sigma_{r\theta} & \sigma_{\theta\theta} \end{pmatrix}. \tag{21}$$

Setting the external force field to zero for simplicity, the force and torque balance equations for the stress components are given by

$$\partial_r (r\sigma_{rr}) + \partial_\theta (\sigma_{r\theta}) - \sigma_{\theta\theta} = 0, \tag{22}$$

$$\partial_r (r\sigma_{r\theta}) + \partial_\theta (\sigma_{\theta\theta}) + \sigma_{r\theta} = 0, \tag{23}$$

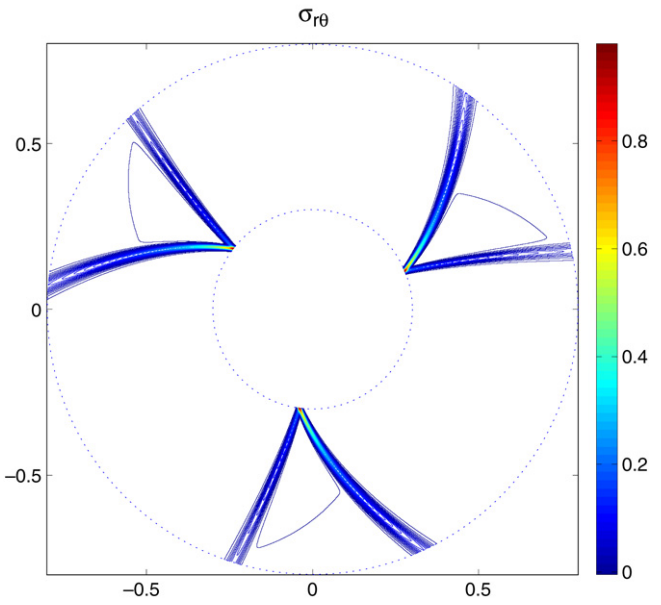

Fig. 5. An example of a stress solution, developing in an annulus of constant fabric tensor under shear. Three localized load sources of $\sigma_{r\theta}$ are applied along the inner boundary, giving rise to three pairs of stress paths. Leakage and spiraling stress paths can be observed for constant fabric tensor.

$$2\tilde{p}_{r\theta}\sigma_{r\theta} - \tilde{p}_{\theta\theta}\sigma_{rr} = \tilde{p}_{rr}\sigma_{\theta\theta}. \tag{24}$$

The fabric components $\tilde{p}_{ij}$ can be written as explicit functions of both the components p_{kl} of the fabric tensor in (5) and θ.

Assuming that $\tilde{p}_{rr} \neq 0$, we can write this system for $\vec{u}$, now defined as $\vec{u} = [\sigma_{rr}, \sigma_{r\theta}]^{\mathrm{T}}$, in the form

$$\partial_r \vec{u} + \partial_\theta (A\vec{u}) = D\vec{u}, \tag{25}$$

with

$$A = \frac{1}{r}\begin{pmatrix} 0 & 1 \\ -\tilde{q}_{\theta\theta} & 2\tilde{q}_{r\theta} \end{pmatrix}, \qquad D = \frac{1}{r}\begin{pmatrix} -1-\tilde{q}_{\theta\theta} & 2\tilde{q}_{r\theta} \\ 0 & -2 \end{pmatrix}.$$

Here, $\tilde{q}_{ij} = \frac{\tilde{p}_{ij}}{\tilde{p}_{rr}}$. This linear system is of similar form as the corresponding system (7) for the Cartesian coordinates. The eigenvalues of the matrix A are

$$\lambda_{1,2} = \frac{1}{r}\left(\tilde{q}_{r\theta} \pm \sqrt{\tilde{q}_{r\theta}^2 - \tilde{q}_{\theta\theta}}\right).$$

The eigenvector y_i, corresponding to λ_i, is given by $y_i = [1, r\lambda_i]^{\mathrm{T}}$. Transforming system (25) into characteristic form, we obtain

$$\partial_r \vec{w} + \Lambda\partial_\theta \vec{w} = (B - \partial_\theta \Lambda)\,\vec{w} + Y^{-1}DY\vec{w}, \tag{26}$$

with $\Lambda = \mathrm{diag}(\lambda_1, \lambda_2)$, and

$$B = \frac{-1}{r(\lambda_1 - \lambda_2)}\begin{pmatrix} \partial_r(r\lambda_1) + r\lambda_1\partial_\theta\lambda_1 & \partial_r(r\lambda_2)_r + \lambda_2\lambda_{2,\theta} \\ -\partial_r(r\lambda_1) - r\lambda_1\partial_\theta\lambda_1 & -\partial_r(r\lambda_2) - r\lambda_2\lambda_{2,\theta} \end{pmatrix}.$$

The equations for w_1 and w_2 are coupled both through the off-diagonal elements of B and through the off-diagonal elements of $Y^{-1}DY$. An inspection of these terms shows that even when the fabric components $\tilde{p}_{ij}$ are everywhere constant, in which case the matrix B vanishes, the characteristic variables may still be coupled due to the off-diagonal terms of $Y^{-1}DY$. We therefore expect leakage to be prevalent in cylindrical geometries even for constant fabric tensors. The dependence of the eigenvectors on θ and r also shows that even for constant fabric components $\tilde{p}_{i,j}$, the stress paths are not straight as in the Cartesian case, but spiral. Such a case is illustrated in Fig. 5 where three narrow Gaussian sources of $\sigma_{r\theta}$ are applied along the inner boundary at r_0, corresponding to a sheared annulus. In this figure, we use a constant fabric tensor $\tilde{P}$ with $\tilde{p}_{rr} = 1$, $\tilde{p}_{r\theta} = 0.2$ and $\tilde{p}_{\theta\theta} = -0.1$.

6. Estimates and perturbation analysis for variable fabric tensors in Cartesian coordinates

In this subsection we analyze the solution for variable fabric tensors by using a perturbation expansion. In particular, we derive an estimate of the solution in terms of the data, and arrive at useful approximations for localized boundary data and slowly varying or locally varying fabric tensors.

Consider the domain given by $X \geq x \geq 0$, $-\infty < y < \infty$. We again assume, for clarity, that the force field $\vec{g} = 0$. The extension to finite $\vec{g}$ is straightforward. As shown previously, the system of stress equations can be written in terms of the characteristic variables $\vec{w}$ as

$$\partial_x \vec{w} + \Lambda \partial_y \vec{w} = -\partial_y \Lambda \vec{w} - B\vec{w}, \qquad B = Y^{-1}\left(\partial_x Y + \partial_y Y \Lambda\right) \tag{27}$$

with $\vec{w}(0, y) = \vec{h}(y) = Y^{-1}\vec{f}(y)$. Rather than analyzing (27) directly, we introduce the expansion

$$\vec{w} = \vec{w}_0 + \vec{w}_1 + \vec{w}_2 + \cdots, \tag{28}$$

and split the matrix B as $B = B_D + \tilde{B}$, with B_D containing the diagonal elements of B and $\tilde{B}$ the off-diagonal elements. We now let $\vec{w}_0$ satisfy the decoupled system

$$\partial_x \vec{w}_0 + \partial_y (\Lambda \vec{w}_0) + B_D \vec{w}_0 = 0, \qquad \vec{w}_0(0, y) = \overrightarrow{h}(y). \tag{29}$$

This decoupled system of equations can be solved directly by integrating each of its components, $w_{0,1}$ and $w_{0,2}$, along the appropriate characteristic path $(x(s), y(s))$, defined in (16), which gives

$$w_{0,i}(x(s_1), y(s_1)) = \mathrm{e}^{-\int_{s_0}^{s_1}\left[\partial_y(\lambda_i) + B_{ii}\right]\mathrm{d}s} h^{(i)}(y(s_0)), \quad i = 1, 2. \tag{30}$$

The change in the characteristic variables $w_{0,i}$ is determined by

$$-\int \left[\partial_y(\lambda_i) + B_{ii}\right]\mathrm{d}s, \quad i = 1, 2. \tag{31}$$

The equations for the remaining terms $\vec{w}_j$ in the expansion take the form

$$\partial_x \vec{w}_j + \partial_y \left(\Lambda \vec{w}_j\right) + B_D \vec{w}_j = -\tilde{B}\vec{w}_{j-1}, \qquad \vec{w}_j(0, y) = 0, \quad j = 1, 2, \ldots. \tag{32}$$

Again, the characteristic variables $w_{j,i}$, $i = 1, 2$ are decoupled, but in contrast to Eq. (29) an additional source term appears on the right-hand side of the equation. It is this source term that indirectly introduces leakage in the expansion series: whereas an isolated boundary load leads to two independent $w_{0,1}$ and $w_{0,2}$ paths, nonzero $w_{0,1}$ and $w_{0,2}$ values along these paths introduce growth of $w_{1,2}$ and $w_{1,1}$ through the source term introduced by $\tilde{B}$ in Eq. (32). Similar behavior is introduced in $\vec{w}_{i+1}$ by $\vec{w}_i$ for $i \geq 1$.

To analyze the convergence of this expansion we consider the remainder

$$\vec{r}_k = \vec{w} - (\vec{w}_0 + \vec{w}_1 + \cdots + \vec{w}_k), \tag{33}$$

which satisfies

$$\partial_x \vec{r}_k + \partial_y (\Lambda \vec{w}_k) + B_D \vec{w}_k = -\tilde{B}\vec{w}_{k-1}. \tag{34}$$

We introduce the bound

$$\eta^k(x) = \max_{y, 0 \leq \xi \leq x} \|\vec{r}_k(x, y)\|. \tag{35}$$

By integrating (33) along the characteristics we obtain

$$\|\vec{r}_k(x, y)\| \leq C(X) \int_0^x \eta^{k-1}(\xi)\mathrm{d}\xi. \tag{36}$$

Here

$$C(X) = b\mathrm{e}^{KX}, \qquad K = \max_{0 \leq x \leq X, y, i}(0, -\partial_y \lambda_i - B_{ii}), \qquad b = \max_{0 \leq x \leq X, y} \|\tilde{B}(x, y)\|. \tag{37}$$

It follows (see for instance Lemma 3.3.4 in Ref. [13]) that

$$\eta^k(x) \leq \frac{C(X)^k x^k}{k!} \max_{0 \leq \xi \leq x} \eta^0(\xi), \tag{38}$$

which goes to zero in the limit of $k \to \infty$ for any $x \leq X$. In fact, we can show convergence for any interval $0 \leq x \leq X < \infty$.

Similarly we can derive an estimate for the full solution in the form

$$\max_{0 \leq x \leq X, y} \|\vec{w}(x, y)\| \leq \max_y \|\vec{h}(y)\| \sum_0^\infty \frac{C(X)^k X^k}{k!}. \tag{39}$$

Note that in the constant coefficient case $C(X) = 0$, and the estimates are sharp, since in that case $\max \|\vec{w}(x, y)\| = \max \|\vec{h}(y)\|$ and $\vec{w} \equiv \vec{w}_0$. If $C(X)X$ is small then the first term in the expansion can be expected to dominate, and the first few terms can be used to analyze the solution. If $C(X)X$ is not small, convergence can be expected to be slow.

We next consider the expansion in a few cases where the leading terms dominate.

Table 1
Relative errors for σ_{xx} at $x = 4$ for 1, 2 and 3 terms in the expansion series

	$\frac{\|\sigma_{xx}-\sigma_{xx,0}\|}{\|\sigma_{xx}\|}$	$\frac{\|\sigma_{xx}-\sigma_{xx,0}-\sigma_{xx,1}\|}{\|\sigma_{xx}\|}$	$\frac{\|\sigma_{xx}-\sigma_{xx,0}-\sigma_{xx,1}-\sigma_{xx,2}\|}{\|\sigma_{xx}\|}$
$\varepsilon = 0.1$	0.0237	0.0044	0.0002
$\varepsilon = 0.5$	0.2354	0.1483	0.0466

6.1. Slowly varying fabric tensor

Assume the equations are scaled such that the length a characteristic path travels in the domain is ~ 1, and that the derivatives of the fabric tensor are small, say $\sim \delta$, $|\delta| \ll 1$. Then, derivatives of the eigenvalues are also small and B, $\partial_y \Lambda \sim \delta$. Clearly the constant in Eq. (38) is $C(X) \sim \delta e^{\delta} \ll 1$, and the expansion converges very rapidly. The first term, $\vec{w}_0$ will be a good approximation to the full solution, indicating that stresses propagated predominantly along the characteristic paths without discernible leakage away from these stress paths. The estimate (39) yields $\|\vec{w} - \vec{w}_0\| \sim \delta$. A more precise approximation is obtained by including the next term in the expansion, $\vec{w}_1$, which is generated by the coupling term on the right-hand side $\left(\tilde{B}\vec{w}_0\right)$. This takes into account the primary leakage. Now the error is $\|\vec{w} - \vec{w}_0 - \vec{w}_1\| \sim \delta^2$.

In Fig. 6, we have computed the approximation to σ_{xx} corresponding to the first term, and both the first and second terms, of the perturbation expansion, respectively, for the same cases as in Fig. 3a, that is with $\varepsilon = 0.1$ in (20). The corresponding derivatives of the fabric tensor are $\sim \varepsilon$. The fabric parameters vary slowly, and we expect the perturbation expansion to converge quickly. Table 1 lists the relative error $\|\sigma_{xx}(x, y) - \sum_{i=0}^{k} \sigma_{xx,i}(x, y)\| / \|\sigma_{xx}(x, y)\|$ at $x = 4$, where $\sigma_{xx,i}$ is the stress corresponding to $\vec{w}_i$. Indeed, the agreement between the approximation given in this figure and the full solution is very good, indicating that primary leakage dominates. Note that the error is approximately multiplied by ε each time a term is added. This behavior of the relative error also holds for $\varepsilon = 0.5$. As expected, more terms are now required to approximate the solution well, as is evident for the errors listed in the table, as well as Fig. 7.

This behavior of the relative error also holds for $\varepsilon = 0.5$, for which Fig. 7 illustrates that in this case indeed more terms are required to approximate the solution well.

6.2. Fabric tensor varies in small region or thin layer

We now assume that P is constant except in a small region $\tilde{\Omega}$, any characteristic path in $\tilde{\Omega}$ has length $s_0 \leq \delta \ll 1$, and in Ω the growth and decay and coupling terms (b and K) are bounded but not small. A perturbation expansion is valid, with $C(X)x \sim \delta b e^{\delta K}$. Clearly, it will converge quickly only if δ is sufficiently small. If a stress path along one characteristic enters $\tilde{\Omega}$, the coupling between the characteristic variables will generate a secondary stress path along the other characteristic. The strength of the secondary path will be proportional to $\delta b e^{\delta K}$. As we will see in the following example, this mechanism can explain the branching phenomena observed in experiments directly from the stress equations. This is in contrast to models of force branching that had to introduce additional assumptions [14].

As an example and for clarity, we analyze branching caused by an isolated thin layer of high-gradient P. Consider a material with a constant fabric tensor, P_1, for $0 \leq x \leq x_0$, and another constant fabric tensor, P_2, for $x_0 + \delta \leq x$. P varies continuously within the thin layer between these regions, $x_0 \leq x \leq x_0 + \delta$, $\delta \ll 1$. Let Y_1 and Y_2 be the eigenvector matrices corresponding to P_1 and P_2, respectively. The solutions in the two constant layers can be expressed with the help of the two sets of characteristic variables, $\vec{w}^{(1)} = (w_1^{(1)}, w_2^{(1)})^{\mathrm{T}}$ and $\vec{w}^{(2)} = (w_1^{(2)}, w_2^{(2)})^{\mathrm{T}}$, as

$$\vec{u}(x, y) = \begin{cases} Y_1 \vec{w}^{(1)}(x, y) & 0 \leq x \leq x_0, \\ Y_2 \vec{w}^{(2)}(x, y) & x_0 + \delta \leq x. \end{cases} \tag{40}$$

Here $w_i^{(j)}$ is constant on characteristic path i within the constant layer j.

To analyze how the middle layer couples the stresses in the two constant layers that it separates, it is convenient to rescale (7) in the x-direction by introducing

$$\tilde{x} = \frac{x - x_0}{\delta}, \qquad u(x, y) = \tilde{u}(\tilde{x}, y),$$

yielding a system in the layer of the form

$$\partial_{\tilde{x}} \tilde{u} + \delta \partial_y (A(\delta \tilde{x} + x_0, y)\tilde{u}) = 0, \quad 0 \leq \tilde{x} \leq 1.$$

A regular perturbation expansion in δ can be performed, showing that $\tilde{u}(\tilde{x}, y)$ varies only slowly with $\tilde{x}$. In particular,

$$u(x_0 + \delta, y) = u(x_0, y) + \mathcal{O}(\delta), \tag{41}$$

which couples the solutions in the two constant layers. There is no difficulty in letting $\delta \to 0$, showing that the limit solution will be continuous at $x = x_0$ even though the limit fabric tensor is discontinuous.

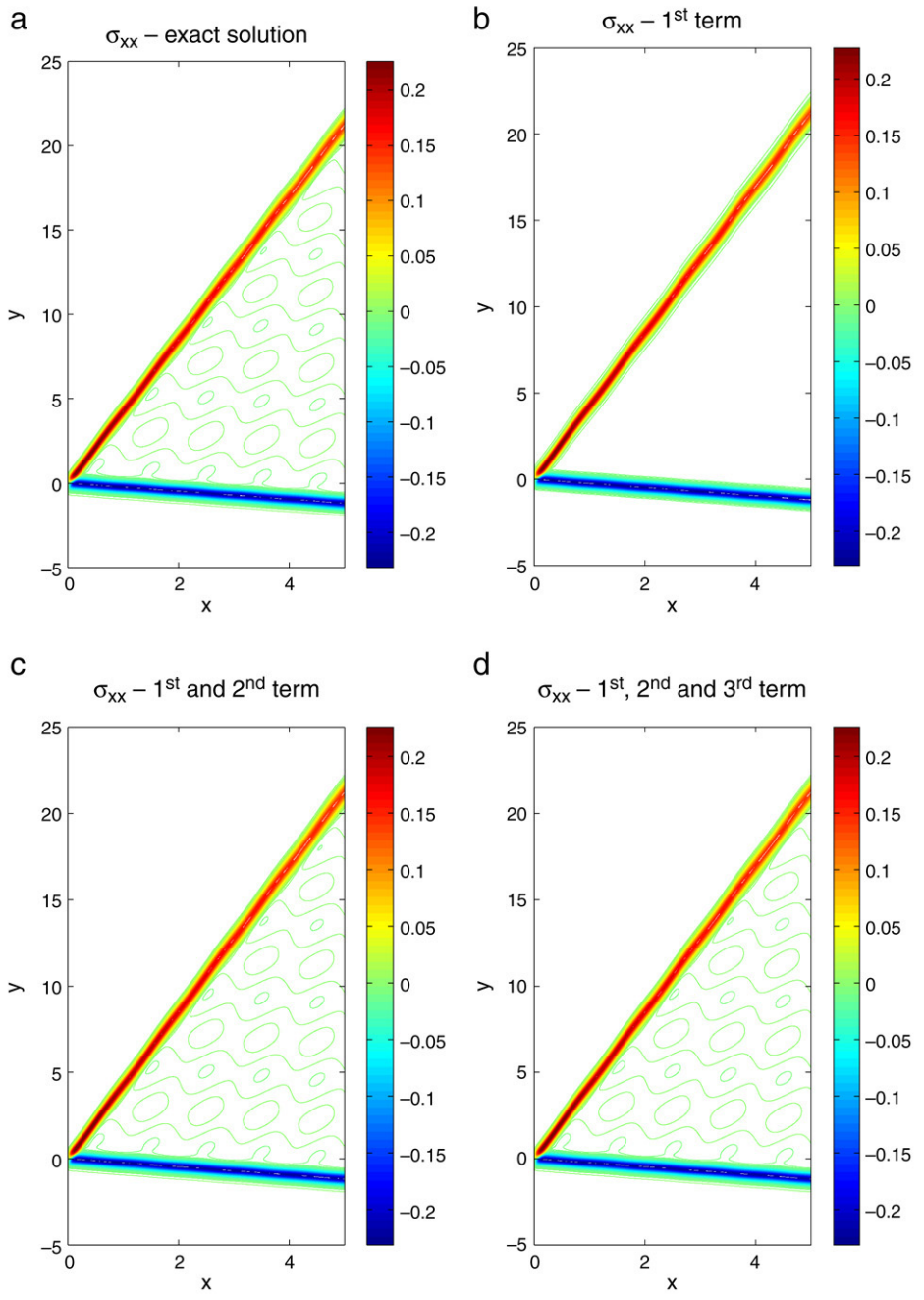

Fig. 6. Contour plots of σ_{xx} for the first two terms in the expansion for the variable fabric tensor given by Eq. (20) with $\varepsilon = 0.1$ when a narrow Gaussian-shaped stress σ_{xx} is applied at (0, 0): (a) Exact solution; (b) first term in the expansion; (c) first and second terms in the expansion; (d) first, second and third term in the expansion.

Now consider a load $\vec{u}(0, y)$ localized around $y = y_0$. In the first layer the solution $\vec{u}$ will consist of stress paths emanating from $(0, y_0)$. On each of these paths only one of $w_1^{(1)}$ and $w_2^{(1)}$ is nonzero. By expressing (41) in terms of the two sets of characteristic variables one obtains

$$\vec{w}^{(2)}(x_0 + \delta, y) = Y_2^{-1} Y_1 \vec{w}^{(1)}(x_0, y) + \mathcal{O}(\delta), \tag{42}$$

where in general $Y_2^{-1}Y_1$ will be a full matrix. Let (x_0, y_s) be a point where one of the stress paths in the first layer reaches the connecting layer. By (42), both $w_1^{(2)}$ and $w_2^{(2)}$ will be nonzero at $(x_0 + \delta, y_0)$, the corresponding point on the other side of the transition layer. This means that two stress paths emanate from $(x_0 + \delta, y_0)$. In other words, branching occurs. In Fig. 8

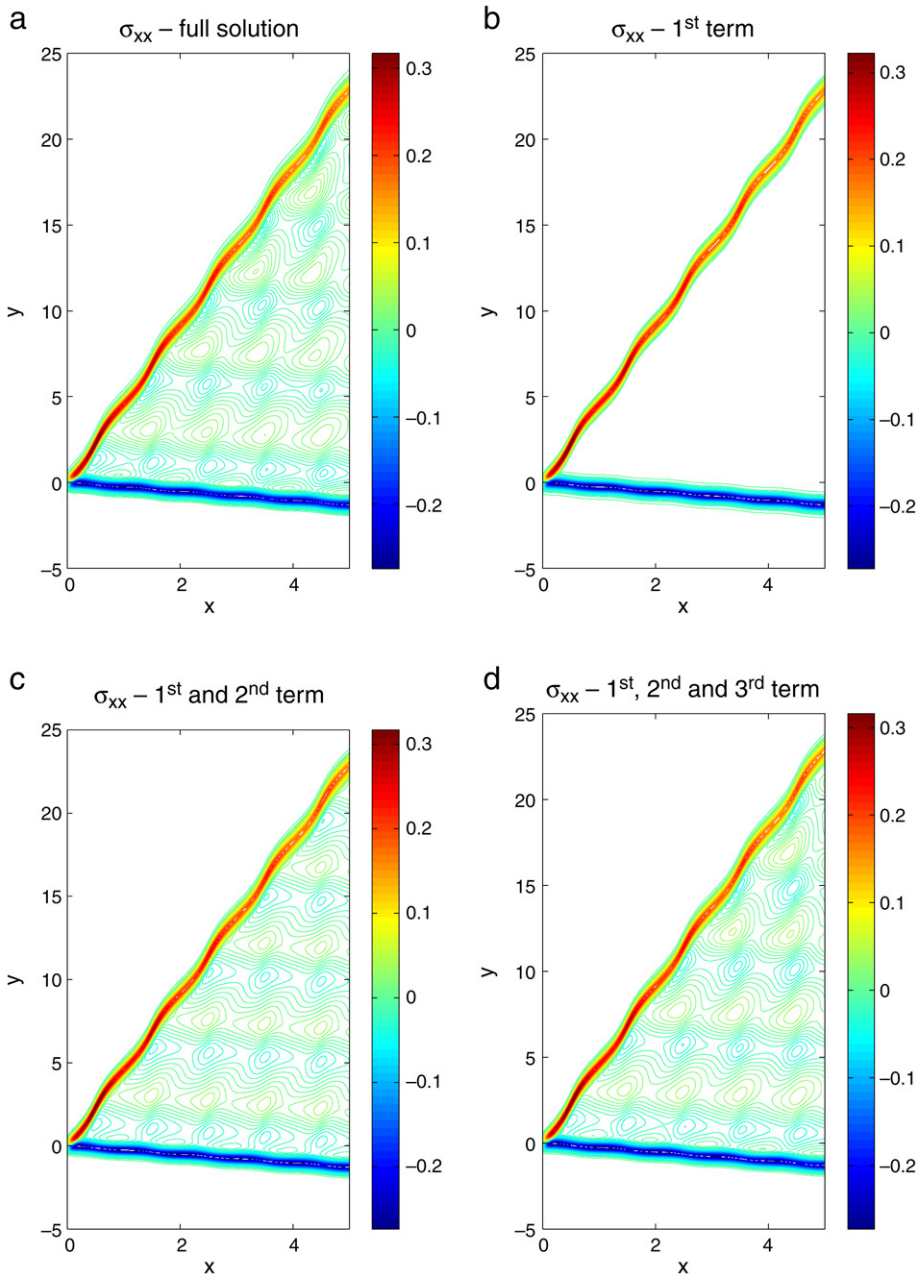

Fig. 7. Contour plots of σ_{xx} for the first two terms in the expansion for the variable fabric tensor given by Eq. (20) with $\varepsilon = 0.5$ when a narrow Gaussian-shaped stress σ_{xx} is applied at (0, 0): (a) exact solution; (b) first term in the expansion; (c) first and second terms in the expansion; (d) first, second and third term in the expansion.

we show three numerical solutions, with $\delta = 0.5, 0.2$ and 0.01, to illustrate the above analysis for a narrow gaussian σ_{xy} centered at (0, 0). We set $x_0 = 1$ and use

$$P_1 = \begin{pmatrix} 2 & 1 \\ 1 & \dfrac{-3}{2} \end{pmatrix}, \qquad P_2 = \begin{pmatrix} 1 & 1 \\ 1 & -3 \end{pmatrix}. \tag{43}$$

In this case the matrix in (42) connecting the two sets of characteristic variables is the full matrix

$$Y_2^{-1} Y_1 = -\frac{1}{8} \begin{pmatrix} 3 & 7 \\ 5 & 1 \end{pmatrix}.$$

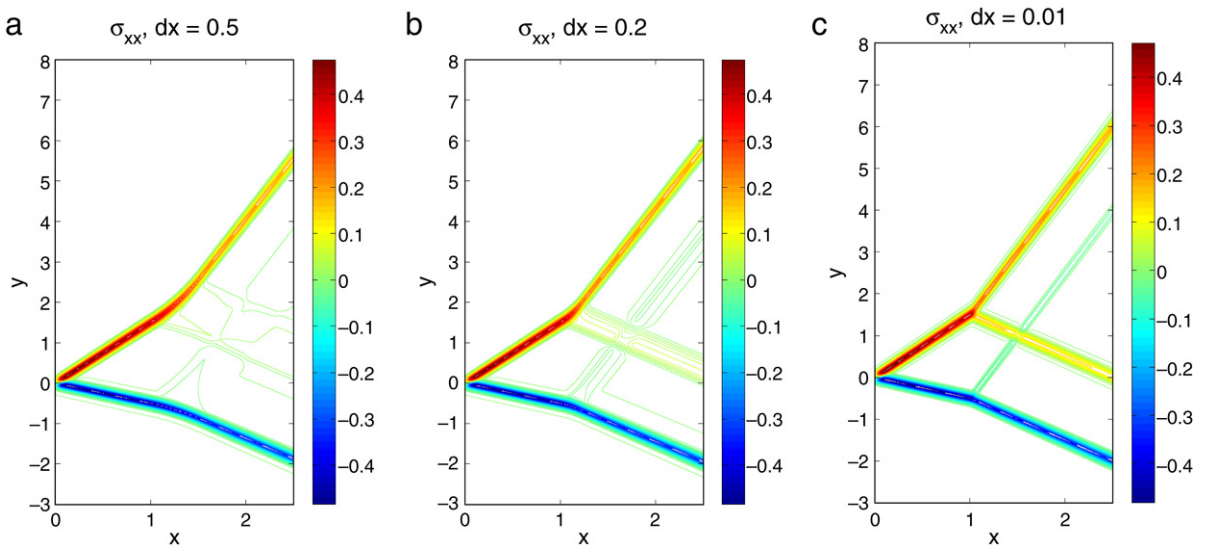

Fig. 8. Contour plots of σ_{xx} for the first two terms in the expansion for the variable fabric tensor given by Eq. (43) when a narrow Gaussian-shaped stress σ_{xy} is applied at (0, 0): (a) $dx = 1$; (b) $dx = 0.1$; (c) $dx = 0.01$.

The fabric tensor in the middle layer varies linearly between the two tensors. To within our numerical accuracy, the solution for $\delta = 0.01$ is indistinguishable from the $\delta = 0$ limit solution.

7. Discussion and conclusions

We have analyzed a recently proposed continuous model for stress fields that develop in two-dimensional isostatic granular systems [9,4]. We have re-formulated the field equations as a linear first-order hyperbolic system and have shown that this form is very convenient both for analysis and for numerical computations. Our analysis reveals wide range of non-uniform stresses, which bear good resemblance to the rich stress patterns observed experimentally, and it makes possible several significant new predictions. In particular, it allows us to predict quantitatively the formation and directions of stress paths and, from these, the trajectories and magnitudes of force chains [3]. We can further predict growth or decay of stresses along the main paths, as well as leakage and branching from the main paths into the cones that they make, in terms of the fabric tensor used to describe coarse-grained geometrical properties of the material. We have carried out numerical computations which verify the analytic results and illustrate the rich behavior that we have discovered.

In the analysis presented here, we have only used synthetic fabric tensors. One reason is that there is very little data at this stage on realistic fabric tensors for isostatic systems. Such data is currently being collected on simulated granular packs. Preliminary results suggest that the distribution of the components of the tensor P is exponential [15]. However, we intend to extract better data on the statistics of the fabric tensor from measurement of real granular materials close to isostatic states that are being currently planned [12]. Another reason is that the artificial fabric tensor which we have selected illustrate clearly the effects of the structural characteristics on the stress patterns.

Our results pave the way to a range for possible future research. One direction consists of tests of our predictions against experimental measurements of fabric tensors and statistics of stress path networks in systems that are very close to isostatic states. Another significant direction is an extension of the analysis to realistic granular systems. As has been mentioned in the introduction, it has been proposed that real systems are non-isostatic, comprising both overconnected and isostatic regions. The simplest way to use this picture is to assume that the overconnected regions respond to loading elastically and model real granular systems as stato-elastic composites: part isostatic and part elastic. Such a theory is yet to be developed, but we hope that the new insights provided by our analysis will make it possible to study more closely such two-phase mixtures. A third line of continued research is to use our static stress solutions to predict dynamics of rearrangement of granular materials under increased loading. In realistic isostatic granular systems there is an yield stress above which the configuration of the system changes. The yield stress defines a surface in the space spanned by the stress components, known as the yield surface. The larger the system the smaller the volume that the yield surface envelopes around zero stresses. On applying a load to the material it reorganizes until it settles into a new mechanical equilibrium, with new fabric parameters. With simple assumptions on this quasi-static dynamics and presuming that the material settles into an isostatic state, it is possible to construct a non-linear model of such behavior. We are currently investigating such a model.

In conclusion,

- a new and very convenient formulation of the continuous stress equations isostatic granular systems has been presented;
- the formulation allowed us to calculate stress paths directly, for both constant and variable fabric tensors, without any need for the full stress solution;

- terms effecting leakage and branching for variable fabric tensors have been identified explicitly and the rich stress patterns that emerge have been shown to be readily analyzable;
- a perturbation analysis has been constructed and demonstrated for the analysis of stress solutions for strongly varying fabric tensors;
- the analysis has been carried out for both popular experimental setups: Cartesian and cylindrical geometries.

Acknowledgements

RB acknowledges funding from EPSRC Grant GR/T28959/01.

References

[1] V.V. Sokolowskii, Statics of Granular Materials, Pergamon Press, Oxford, 1965;
R.L. Brown, J.C. Richards, Principles of Powder Mechanics, Pergamon, NY, 1966;
R.M. Nedderman, Statics and Kinematics of Granular Materials, Cambridge University Press, Cambridge, 1992;
H.M. Jaeger, S.R. Nagel, R.P. Behringer, Rev. Modern. Phys. 68 (1996) 1259.
[2] S. Luding, Phys. Rev. E 55 (1997) 4720;
L.E. Silbert, G.S. Grest, J.W. Landry, Phys. Rev. E 66 (2002) 061303;
J.H. Snoeijer, T.J.H. Vlugt, M. van Hecke, W. van Saarloos, Phys. Rev. Lett. 92 (2004) 054302;
S. Ostojic, E. Somfai, B. Nienhuis, Nature 439 (2006) 828.
[3] L. Vanel, D.W. Howell, D. Clark, R.P. Behringer, E. Clement, Phys. Rev. E 60 (1999) R5040;
A.P.F. Atman, P. Brunet, J. Genbg, G. Reydellet, P. Claudin, R.P. Behringer, E. Clement, Eur. Phys. J. E 17 (2005) 93.
[4] R. Blumenfeld, Phys. Rev. Lett. 93 (2004) 108301.
[5] R. Blumenfeld, New J. Phys. 9 (2007) 160.
[6] R.C. Ball, in: M. Lal, R.A. Mashelkar, B.D. Kulkarni, V.M. Naik (Eds.), Structures and Dynamics of Materials in the Mesoscopic Domain, Imperial College Press, London, 1999.
[7] R. Blumenfeld, in: Maria-Carme T. Calderer, Eugene M. Terentjev (Eds.), Modeling of Soft Matter, in: IMA Volume in Mathematics and its Applications, vol. 141, Springer-Verlag, 2005, pp. 235–246. cond-mat/0501700.
[8] J.P. Wittmer, P. Claudin, M.E. Cates, J.-P. Bouchaud, Nature 382 (1996) 336;
J.P. Wittmer, M.E. Cates, P. Claudin, J. Phys. I (France) 7 (1997) 39;
M.E. Cates, J.P. Wittmer, J.-P. Bouchaud, P. Claudin, Phys. Rev. Lett. 81 (1998) 1841.
[9] R.C. Ball, R. Blumenfeld, Phys. Rev. Lett. 88 (2002) 115505.
[10] R. Blumenfeld, Physica A 336 (2004) 361.
[11] C.-W. Shu, S. Osher, Efficient implementation of essentially nonoscillatory shock-capturing schemes, J. Comput. Phys. 77 (1988).
[12] R.P. Behringer, private communication.
[13] H.-O. Kreiss, J. Lorenz, Initial-boundary value problems and the Navier–Stokes equation, Academic Press, Boston, 1989.
[14] C. Liu, et al., Science 269 (1995) 513;
J.-P. Bouchaud, R.P. Behringer, C. Veje, Phys. Rev. Lett. 82 (1999) 5241;
M.E. Cates, J.P. Wittmer, J.-P. Bouchaud, P. Claudin, Phys. Rev. Lett. 81 (1998) 1841;
D. Howell, R.P. Behringer, C. Veje, Phys. Rev. Lett. 82 (1999) 5241.
[15] G. Frenkel, R. Blumenfeld, Z. Grof, P.R. King, Phys. Rev. E 77 (2008) 041304.